Delft University of Technology

Chemical deformation of metakaolin based geopolymer

Li, Zhenming; Zhang, Shizhe; Zuo, Yibing; Chen, Wei; Ye, Guang

Important note
To cite this publication, please use the final published version (if applicable).
Please check the document version above.

Chemical deformation of metakaolin based geopolymer

Zhenming Li[a], Shizhe Zhang[a], Yibing Zuo[a], Wei Chen[b,c,*,] and Guang Ye[a,*]

[a]Department of Materials and Environment (Microlab), Faculty of Civil Engineering and Geoscience, Delft University of Technology, Delft, the Netherlands

[b]School of Materials Science and Engineering, Wuhan University of Technology, Wuhan, China

[c]State Key Laboratory of Silicate Materials for Architecture (Wuhan University of Technology), Wuhan, 430070, China.

E-mail: Z.Li-2@tudelft.nl
Shizhe.Zhang@tudelft.nl
Y.Zuo@tudelft.nl
Chen.wei@whut.edu.cn
G.Ye@tudelft.nl

* Corresponding author

Abstract:

Chemical deformation (chemical shrinkage/expansion), the absolute volume change during reactions, is a key parameter influencing the volume stability, especially the autogenous deformation of a binder material. This work, for the first time, reports an in-depth investigation on the chemical deformation of metakaolin based geopolymer (MKG). Unlike ordinary Portland cement-based binders with monotonic chemical shrinkage, MKG experiences three stages of chemical deformations: chemical shrinkage in the first stage, chemical expansion afterward and chemical shrinkage again in the final stage. Various experimental techniques (XRD, FTIR and NMR) plus theoretical calculations are applied to explore the mechanisms behind the chemical deformation of MKG. Clear correlations are found between the chemical deformations and the reaction processes during geopolymerization. A conceptual chemical deformation model for geopolymer is summarised. The insights into the chemical deformation provided by this study will play a fundamental role in further understanding, controlling and even utilizing the deformation behaviours of geopolymers.

Keywords: chemical shrinkage, chemical expansion, volume change, metakaolin, geopolymer

1. Introduction

Geopolymer is a class of inorganic polymer binder typically synthesized via alkaline activation of aluminosilicate precursors [1]. This material has attracted increasing interest in last decades, due to its promising potential to be used as an alternative binder to ordinary Portland cement (OPC). Even though OPC has been widely used for centuries with superior engineering performances, the OPC production contributes 5-8% of CO_2 emission worldwide [2]. Geopolymers, on the other hand, are mainly made

from industrial by-products or other inexpensive aluminosilicate materials and the production of geopolymers usually induces much less environmental footprint [3]. Many studies have been conducted to explore the physical/chemical properties and long-term performance of geopolymers. It has been reported that geopolymers can show high strength, excellent thermal resistance and very good durability [4–6]. However, the volume stability, especially the bulk deformation of geopolymers remains an unsolved issue, which has largely hindered the application of this material in engineering practise [7–9].

Ma et al. and Li et al. investigated the autogenous shrinkage of fly ash based geopolymer (FG) and metakaolin based geopolymer (MKG), respectively [8,9] Although autogenous shrinkage was observed in their studies, the internal relative humidity of the mixtures didn't decrease, which serves as strong evidence that the autogenous shrinkage of FG and MKG cannot be explained by the classical self-desiccation theory for OPC. In addition, some researchers observed expansion of FG, MKG and their blended systems at certain curing ages when the samples were cured in sealed or humid conditions [10–13]. Such expansion cannot be explained by the theories for OPC either, of which the expansion is normally attributed to the formation of ettringite or the sucking back of bleeding water. To explain the deformation behaviours of geopolymers, research on the chemical deformations is crucial.

Chemical deformation is the absolute volume change of a binder material associated with the chemical reactions and it is the key factor influencing the volume change of the materials [14,15]. For OPC, the theoretical chemical deformation associated with cement hydration was already established through experimental and modeling methods [16,17], which provides important information for researchers and engineers to estimate the autogenous shrinkage and drying shrinkage. The chemical deformation associated with geopolymerization, however, has seldom been studied, thus hindering a better understanding towards deformation behaviours of geopolymers.

The purpose of this study, therefore, is to investigate the chemical deformation of geopolymer and try to clarify the mechanisms behind. In the first step, the evolution of chemical deformation of MKG paste was measured and discussed. Secondly, the reaction processes corresponding to the chemical deformation were investigated by intensive characterization of MKG pastes cured at different ages. A correlation was established between the chemical deformation and reaction process. Moreover, the reason why different reaction processes result in different chemical deformations is qualitatively/semi-quantitatively interpreted based on experimental results and/or theoretical calculations. In the end, a conceptual model of chemical deformation of geopolymerization for MKG is presented.

2. Materials and methods

2.1 Materials

MK and fly ash are the two most common used precursors to synthesize geopolymer. MK, in particular, is widely used as a model material in laboratory to study geopolymerization, because it is purer and more homogenous than fly ash which contains lots of impurities and hollow voids inside. The most commonly used compounds for alkali activator are MOH and $M_2O \cdot rSiO_2$, where M is either Na or K [18]. Hence, in this study MK is used as precursor and $NaOH/Na_2SiO_3$ solution is selected as activator to synthesize geopolymer paste. The MK was from Caltra Nederland B.V. with a d_{50} particle size of 11.5 μm and density of 2.2 g/cm^3. The chemical composition of this material was determined by means of X-ray fluorescence spectrometry (XRF) as shown in Table 1.

The reactive SiO_2 and Al_2O_3 contents in MK were determined by chemical dissolution method. The MK was dissolved in dilute hydrochloric acid solution and was afterwards treated with boiling sodium carbonate solution [19]. The obtained residue was rinsed, heated up to 950 °C and then was cooled to room temperature in a desiccator before subject to XRF test. The dissolved fraction corresponding to the mass loss after chemical dissolution treatment is determined as the amorphous phase content. The amount of reactive SiO_2 and Al_2O_3 is shown in Table 1 and Table 2. The molar ratio of Si/Al of the reactive part of MK is 0.76. The density of the amorphous part of MK determined by pycnometer method is 2.08 g/ml, which is a bit lower than the overall density of MK.

Table 1

Chemical composition of MK and its insoluble residue

Oxide (wt. %)	SiO_2	Al_2O_3	CaO	Fe_2O_3	K_2O	TiO_2	ZrO_2	Other
MK	45.35	47.49	0.20	0.63	0.06	1.64	0.11	2.51
I.R.	60.87	26.00	0.16	0.81	0.35	10.78	0.79	0.23

I.R. = insoluble residue

Table 2

Reactivity of MK (wt. %).

Components	I.R.	Reactive content	Total SiO_2	Reactive $SiO2$	Total Al_2O_3	Reactive Al_2O_3
Weight (%)	13.17	86.83	47.49	39.47	47.35	43.93

I.R. = insoluble residue

The alkaline activator was prepared by mixing sodium hydroxide pellets (analytical grade, >98 % purity) with distilled water and sodium silicate solution (Na_2O: 8.25 wt. %, SiO_2: 27.50 wt. %). The solution was then allowed to cool for 24 hours before sample preparation. The mixture design of the investigated MKG paste is presented in Table 3. The overall Si/Al of the paste is 1.15.

Table 3

Mixture proportions of MKG paste.

Reactants	SiO_2 (mol)	Al_2O_3 (mol)	Na_2O (mol)	H_2O (g)
MK	1.97	1.29	--	--
Activator	1	--	1.5	350
total	2.97	1.29	1.5	350

An OPC paste with water/cement ratio of 0.4 was used as a reference sample in section 3.1. The cement type was CEM I 52.5 N from Gaurain and the chemical composition of the cement was shown elsewhere [9].

2.2 Methods

2.2.1 Testing method for chemical deformation

The testing method of chemical deformation of MKG paste was adapted from the gravimetry method or so-called buoyancy method for Portland cement [20,21]. The detailed experimental set up is illustrated in Fig. 1.
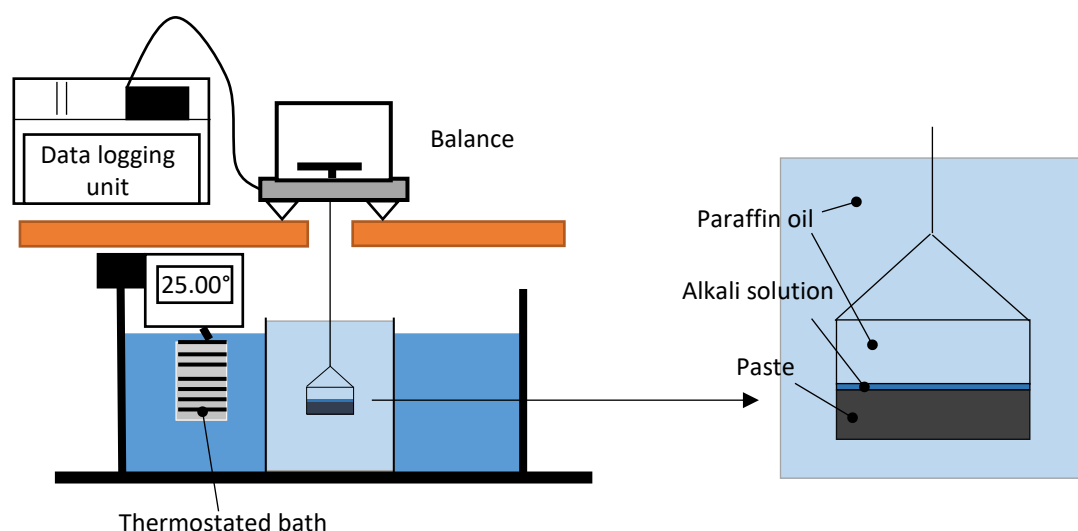

Fig.1 Schematic of devices for chemical shrinkage measurement, after [21].

According to mixture proportion, 100 g of MK was mixed with alkali solution in a container using a small blender for 4 minutes. Then, around 100 grams of paste was poured into a plastic vessel with a diameter of 8 cm. Glass container was not chosen because it may react slowly with the alkali solution. A thin layer (around 10 grams) of alkali solution with the same concentration as activator was gently added onto the surface of the paste by pipette. The amount of liquid should be sufficient to cover the entire surface of paste and also to compensate the chemical shrinkage, but in the meantime, it should be kept as little as possible to diminish the influence on the reaction kinetics of the paste. Paraffin oil was gradually added onto the surface of the alkali solution until the dish was nearly filled. After that, the vessel was gently lowered into a bigger beaker full of paraffin oil. The beaker was placed in the thermostat water

bath at least 1 day in advance of the measurement to equilibrate the temperature. The beaker was used to protect the dish from the disturbance of circulating water and meanwhile to transfer the heat. The temperature of the circulating water in the bath was controlled at 25±0.01 °C. The submerged weight of the sample was recorded automatically every 5 minutes from the time the specimen was placed in the bath (around 20 minutes after casting). The chemical deformation was calculated according to equation 1 [22].

$$V_{CD} = \frac{\Delta V_{paste}(t)}{g_{mk}} = \frac{W_{sub}(t) - W_{sub}(0)}{\rho_{par} \cdot g_{mk}} \qquad (1)$$

Where V_{CD} (ml/g) is the chemical deformation of the paste per gram of MK, ΔV_{paste} (ml) is the volume change of the paste, g_{mk} (g) is the mass of MK, $W_{sub}(t)$ (g) is the submerged weight of the paste at time t, $W_{sub}(0)$ (g) is the initial submerged weight of the paste, and ρ_{par} (g/ml) is the density of the paraffin oil in the buoyancy bath (0.85 g/ml at 25°C). Three replicate samples were measured. The chemical deformation of OPC paste was measured with the same method as MKG paste.

2.2.2 Characterization of MK and MKG pastes

The MKG pastes were ground into powders and the reaction was stopped by solvent exchange method recommended by previous studies [23]. MK and MKG paste powdered samples were characterized by Fourier transform infrared spectroscopy (FTIR), X-ray diffraction (XRD) and magic-angle spinning nuclear magnetic resonance (MAS NMR). FTIR was performed using a Spectrum TM 100 Optical ATR-FTIR spectrometer over the wavelength range of 600 to 4000 cm^{-1} with a resolution of 4 cm^{-1}. XRD was conducted using a Philips PW 1830 powder X-ray diffractometer, with Cu Kα (1.5406 Å) radiation, tube setting to be 40 kV and 40 mA, a step size of 0.030°, and a 2θ range of 5–70°. Solid-state MAS NMR spectra were acquired using a Bruker Avance 400WB spectrometer. The ^{29}Si NMR spectra were collected at 79.5 MHz on a 7 mm probe, with a pulse width of 6.5 μs, a spinning speed of 15.9 kHz and a relaxation delay of 10 s. [24]. The ^{29}Si MAS NMR spectra were deconvoluted into individual Gaussian peaks assigned to different atomic environments of Si according to the literature which have similar chemical environments to this study [23–26]. Aiming for the best fit with highest R^2 value, the peak positions and widths were held constant throughout the deconvolutions of all spectra and the minimum possible number of peaks was used for all spectra deconvolution to ensure an accurate and meaningful interpretation of the spectra [27]. During deconvolution, MK is considered to consist of only Q^4 groups, while the MKG pastes can contain Q^0, Q^1, Q^2 and Q^3. It is assumed that the Q^3(1Al) is the only Q^3(mAl) group due to the high Al content in the samples. The overall Si/Al ratio calculated from the individual peaks was compared with the nominal reactive Si/Al of the mixture to check the correct interpretation of the spectra.

2.2.3 Measurement of volume change associated with dissolving of MK

In order to investigate the volume change associated with MK dissolution, 30 g of MK was mixed with 1000 g of NaOH solution in a conical flask stirring continuously. The volume change during the dissolution process was measured according to dilatometry or so-called Le Chatelier method [20]. The NaOH solution had the same Na_2O content as the activator to provide a similar dissolution environment. SiO_2 was excluded to avoid additional volume change induced by its reaction with the dissolved Al from MK and thus induce additional volume change. 30g of MK was believed to be an optimum in this experimental set up taking account of the balance between accurate acquisition of the volume change and a limited polymerization of dissolved silicate and aluminate species. Considering the very high reactivity of MK under alkaline environment, it was assumed all the reactive contents of MK were dissolved during the tests and no polymerization occurred. The final volume change was recorded when the volume of the system equilibrated after mixing for 5 hours. The test was repeated for 3 times to ensure the reproducibility of the results and the average value of the results was used. The volume change (ml/g) was normalized by dividing the measured volume change (ml) by the mass of investigated MK (g).

3. Results and discussion

3.1 Chemical deformation of MKG paste

The evolution of chemical deformation of MKG paste is presented in Fig.2 (a), with a representative curve shown in solid line and the other two in grey dashed lines. After two weeks of curing, the chemical shrinkage continuously went on only with a decreasing speed. Therefore, only the chemical deformation evolution during the first 14 days is presented. As a reference, the chemical deformation of OPC paste is shown in Fig. 2 (b).
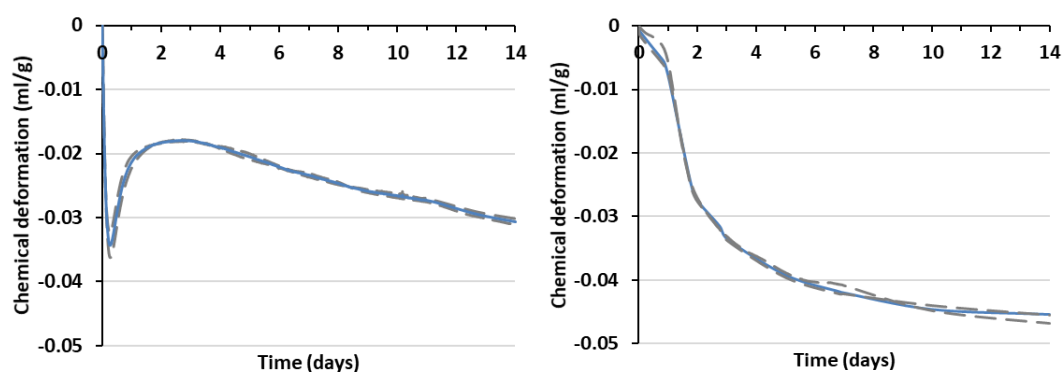

Fig. 2. Chemical deformation of (a) MKG paste, and (b) OPC paste. A representative curve is shown in solid line while the other two curves are shown in grey dashed lines. The curves indicate a good repeatability of the measurement.

It can be seen that the evolution of chemical deformation of MKG is essentially different from that of OPC, which shows monotonic chemical shrinkage after casting [28,29]. MKG firstly experiences a chemical shrinkage process, followed by a chemical expansion in the second stage and a chemical shrinkage again in the final stage. The history of the volume change of MK based geopolymer caused by chemical reaction suggests that the terminology 'chemical deformation' is more proper to describe the volume change associated with geopolymerization rather than the term 'chemical shrinkage' which is commonly used for OPC to describe the absolute volume decrease along the cement hydration.

The multiple-stage development of chemical deformation of MKG is believed to be due to the complexity of geopolymerization. Previous researchers have proposed several models regarding the mechanisms for geopolymerization [30–36]. From the volumetric change point of view, three stages can be observed for the MKG paste as shown by Fig.2. Building up relationships between the volumetric changes with the corresponding reaction products could be a feasible approach to reveal mechanisms of the chemical deformation of MKG related to different stages of geopolymerization. To this end, the precursor MK and MKG pastes cured for 4 hours, 8 hours, 16 hours, 48 hours and 240 hours were characterized by means of FTIR, XRD and NMR. The sample at different curing age are referred to as MK, 4h, 8h, 16h, 48h and 240h, respectively.

3.2 Characterization of MK and reaction processes of MKG paste

3.2.1 FTIR analysis

The FTIR spectra of MK and MKG pastes are presented in Fig.3. In the spectrum of MK, the broad band centered at around 1056 cm^{-1} is assigned to the asymmetric stretching vibration of Si-O-T bonds (T= tetrahedral Si or Al) and the small bump at 1200 cm^{-1} represents the asymmetric stretching of Si-O-Si in the mullite-like structures [37]. Both of these peaks become less apparent at 4 hours indicating that the precursor was largely dissolved at this stage. The main band of the spectrum at 948 cm^{-1} at 4h suggests that an N-A-S-H gel framework was being generated [38]. The small peak at 880 cm^{-1} (marked by the arrow) can be assigned to either the bending vibration of Al-O-H [39,40] or the bending vibration of small anionic species such as silicate monomer, SiO^{-} [41–43]. Since the raw material is undergoing rapid dissolution in this period, the formation of small silicate monomers is believed to be the case here.
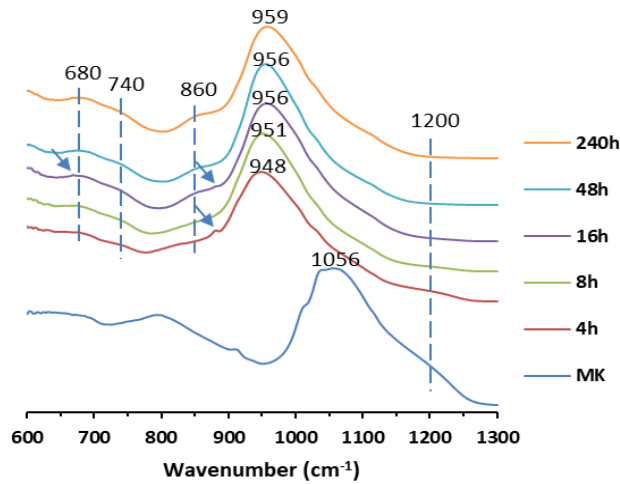
Fig.3. FTIR spectra of MK and MKG pastes.

The main band of spectrum 8h shifts to higher wavenumber as a result of a higher degree of polymerization of the reaction products [44]. In the meantime, the small peak at 880 cm^{-1} is absent, indicating the consumption of silicate monomers in favour of larger species. The main band of the spectrum 16h shifts further to around 956 cm^{-1} indicating the formation of polymerized structures. The humps at around 740 cm^{-1} and 860 cm^{-1}, which are associated with the symmetric stretching and asymmetric stretching vibrations of Al-O bonds in AlO$_4$ tetrahedral groups, respectively, become apparent at this age [45]. The hump at 680 cm^{-1} could also be assigned to the vibration of Al-O bonds [46]. These signals indicate that an increasing amount of Al is incorporated into the structures after 16 hours of curing. The region from 630 cm^{-1} to 760 cm^{-1} generally corresponds to units such as the aluminosilicate ring and cage structures, and the peak at 668 cm^{-1} (marked by the arrow), although not intensive, could indicate the presence of secondary building units or fragments of zeolites [47,48]. The spectrum of sample 16h also exhibits a small peak at 880 cm^{-1}. Since the sample has been cured for 16 hours, this peak is unlikely to be assigned to monomers. According to Watling [40], the peak at 880 cm^{-1} is best assigned to the bending vibration of Al-O-H in a polymeric structure, in which 4-coordinate aluminium atoms are linked by oxygen bridges but are also bonded to unshared hydroxyl groups. The Al-O-H can be the edge of structure units (such as the secondary building units of zeolites) formed in this stage [49,50].

In the spectrum of sample 48h and 240h, the peak at 880 cm^{-1} disappears and the humps around 680 cm^{-1}, 740 cm^{-1} and 860 cm^{-1} become more intensive. This information together with the further shift of the main band towards high wavenumbers indicates the formation of a more polymerized aluminosilicate structure.

3.2.2 XRD analysis

The XRD data collected for precursor powder and geopolymer binders are illustrated in Fig.4.

MK is mainly amorphous, coherent with the high reactivity of this material as shown in section 2.1. The crystals identified in MK are kaolinite-1 *Md* ($Al_2Si_2O_5(OH)_4$, pdf 29-1488), mullite ($Al_2(SiO_4)O$, pdf 83-1510) and with a minor presence of quartz (SiO_2, pdf 83-0539). Some peaks disappear after alkali activation, indicating that some crystals were partly dissolved during reaction [51]. The broad hump displayed in the pattern of MK at about 20°-25° 2θ is typical of aluminosilicate glasses [50]. This hump becomes much less obvious in the patterns of MKG pastes, indicating a fast dissolution of raw material during the first hours of activation.
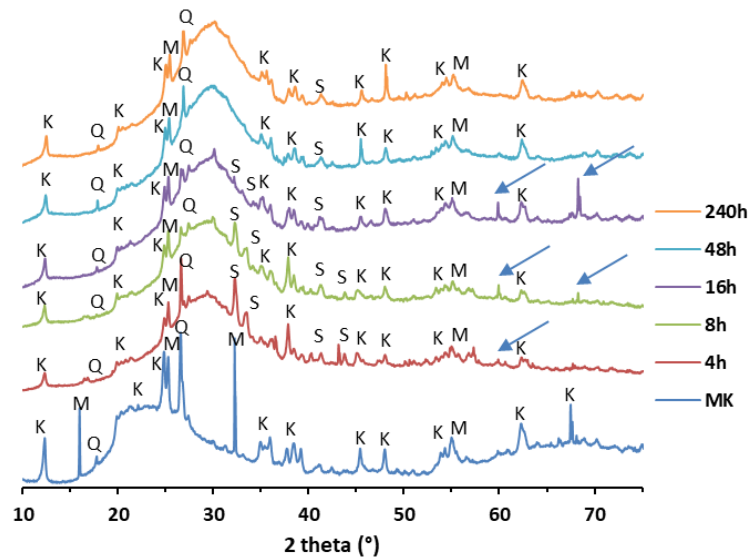

Fig.4. XRD patterns of MK and MKG pastes (K = kaolinite-1 *Md*; M = mullite; Q = quartz; S = sodium carbonates).

The XRD patterns of MKG pastes in general exhibit humps at around 29° 2θ associated with the formation of an N-A-S-H type gel [36,52–54]. The peaks at around 30.27°, 32.1°, 34.2°, 37.9°, 40.2°, 41.3° and 46.6° 2θ in the patterns are attributed to sodium carbonates (Na_2CO_3, pdf 01-075-6816), due to possible carbonation during the sample preparation.

Two new peaks are found at 59.9° 2θ and 68.3° 2θ (marked by arrows) in the pattern of the sample 8h, and the intensity of these peaks increases in the sample 16h. Actually, in the pattern of the sample 4h, the peak at 59.9° 2θ has already appeared just in a lower strength. This indicates that new types of crystalline phases were under formation from 4h up to 16h of curing. These crystals are most likely to be assigned to zeolites, as also found by other researchers in geopolymers [55,56]. Through transmission electron microscope (TEM), Yip et al. observed some zeolitic phases as constituents of the geopolymeric products [56]. Trinepheline ($NaAlSiO_4$, pdf 31–1267) might be the crystal formed here [57]. The areas of peaks 59.9° 2θ and 68.3° 2θ 2θ are small compared with the big hump in the XRD pattern, indicating that the zeolite(s) observable by XRD occupies only a small part of the total reaction products. The main reaction products in sample 8h and 16h are amorphous geopolymer gels or nano-/quasi- crystals that cannot be observed by XRD. In literature, it has been stated that "a significant component of the binder phase formed in geopolymerization is likely to

be comprised of nanometer-sized crystalline structures" [50]. These initially formed zeolites and gels or nano-crystals may act as nuclei for the growth of future reaction products [50].

It is worth noting that the signals of peaks 59.9° 2θ and 68.3° 2θ (marked by arrows in Fig. 4) diminish in the sample 48h and 240h corresponding to the chemical shrinkage at the third stage in Fig. 2. This indicates that the zeolites may be decomposed in this stage and the new products contributed by the species from the decomposition are not long-term ordered and have amorphous structures.

3.2.3 NMR analysis

The ^{29}Si NMR spectra of MK and MKG pastes are presented in Fig.5. It can be seen that the MK has a big hump from -90 ppm to -120 ppm due to the large content of highly polymerized Si groups. The intensity of this hump is significantly reduced after alkali activation. This is in good agreement with the dissolution demonstrated by the FTIR and XRD results. With increasing of curing time, the main bands keep moving to higher chemical shifts and the relative intensity of the regions from -60 ppm to -80 ppm decrease. This is indicative of a decreasing amount of low polymerized species from monomers to small oligomers in favour of more polymerized products. From 48h to 240h, there is only a slight movement of the curves indicating a stable Si coordination environment was formed. The main bands of spectra for MKG pastes, although different in positions, all lie in the region from -83 ppm to -86 ppm, indicating a high Al substitution in the reaction products after activation [24]. This is due to the high overall Al/Si ratio of the mixtures.
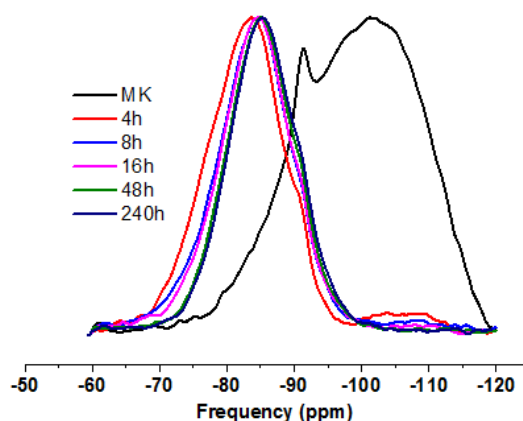

Fig. 5. ^{29}Si NMR spectra of MK and MKG pastes.

To obtain more specific information on Si coordination environments in the reaction products, deconvolution of the curves is conducted. According to literature, the peaks at −76, −79, -82, -84.5, -88, -95, −101.5, −108 ppm are assigned to Q^0, Q^1, Q^2(1Al), Q^4(4Al), Q^4(3Al)/Q^3(1Al), Q^4(2Al), Q^4(1Al), Q^4(0Al), respectively [24,25,58], where the Q^n(mAl) represents the tetrahedral of Si. The narrow peak at -91.5 ppm is due to the presence of kaolinite from the precursor [26]. The peak at -88 ppm is assigned to both Q^3(1Al) and Q^4(3Al) sites due to their overlapping resonance [25,58]. The widths of

different peaks at half-height are between 9 ppm and 12 ppm [24], except for the peak at -91.5 ppm which is 2.3 ppm in width [26].

The deconvolution results and relative quantification of each species at all time points are shown in Fig.6 and Fig.7, respectively. The Si/Al ratios of sample 4h, 16h, 48h and 240h calculated from the deconvoluted results are 1.38, 1.19, 1.17 and 1.18, respectively. These values, especially those for the samples cured for longer times when less MK remained undissolved, are very close to the overall Si/Al ratio (1.15) of the paste, which indicates a sound interpretation using spectra deconvolution.
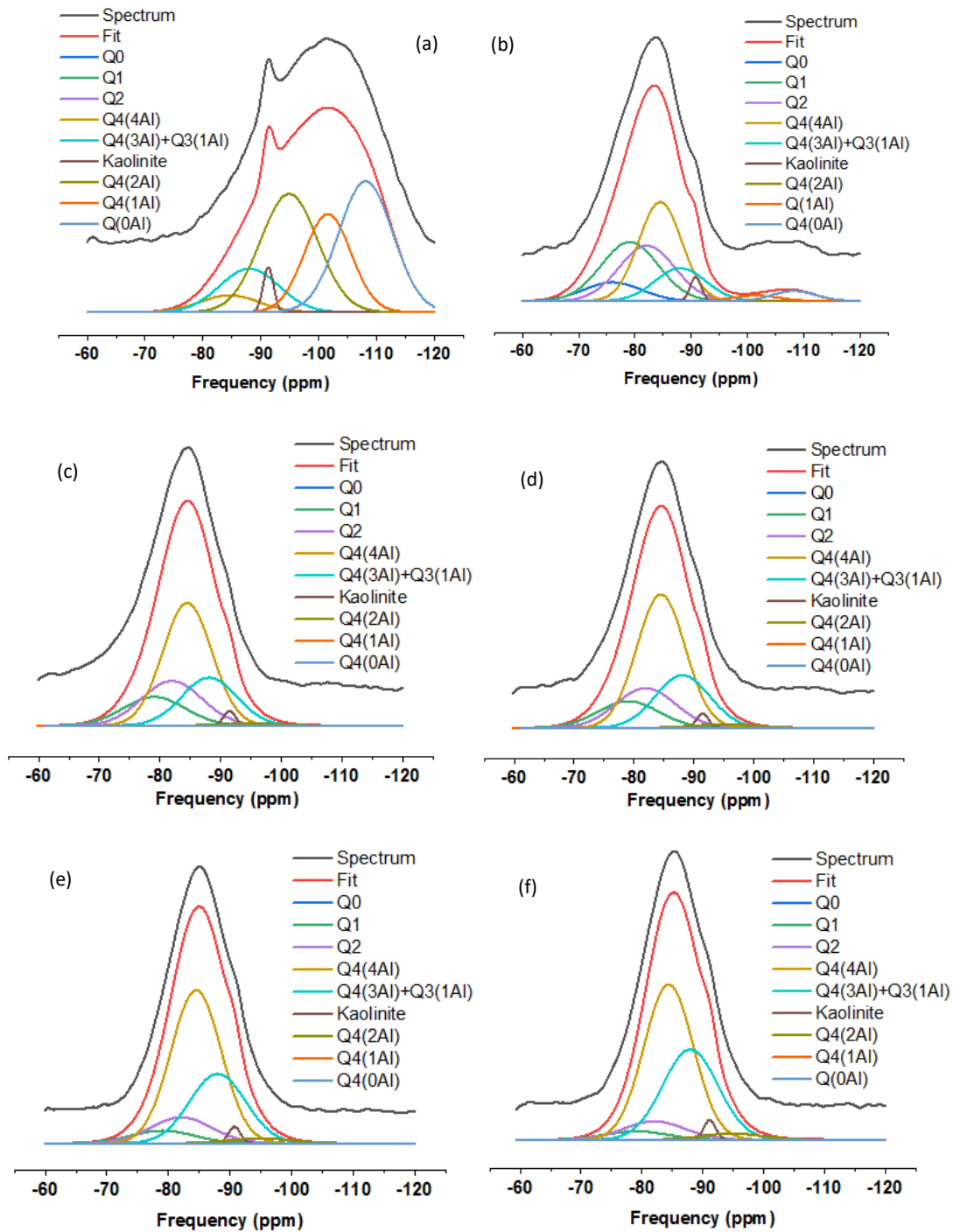
Fig. 6. Deconvolution results for ^{29}Si NMR spectra of MK (a) and MKG pastes cured for 4 hours (b), 8 hours (c) 16 hours (d), 48 hours (e) and 240 hours (f).
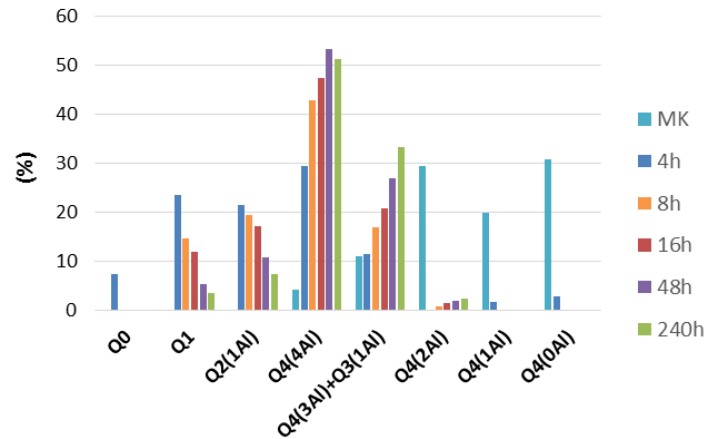

Fig.7. Normalized summary of Qn(mAl) Si coordination environments within MK and MKG pastes identified in the deconvoluted ^{29}Si NMR spectra.

Different stages of MKG reactions could be revealed by the 29Si NMR spectra deconvolution shown in Fig.6 and normalized Si coordination environments Q^n(mAl) in Fig.7. The amounts of Q^4(1Al) and Q^4(0Al) largely decrease up to 4h and lots of Q^0, Q^1, Q^2 species were present, from either the activator or the dissolution of raw material, which indicates the sample was mainly experiencing dissolving process in this period.

In the spectrum of 8h and 16h, the broad bump from -95 ppm to -110 ppm becomes nearly invisible, indicating the dissolution was nearly complete. In the meantime, a large amount of Q^4(4Al) was formed at the expense of consumption of lower polymerized species (Q^0, Q^1, and Q^2(1Al)) in this period. The result is in line with the FTIR spectrum of 16h which shows a large extent of aluminium incorporation in structures. The Q^4(4Al) formed in this period corresponds to the well-known "Al-rich" gels or "gel 1" reported by many researchers as the first stage reaction products in geopolymerization [36,59]. However, as indicated by the XRD and FTIR results, it seems that at least a significant amount of these Al-rich products was (semi-)crystalline zeolites or nano-zeolites rather than completely amorphous gels [50].

The amount of Q^4(4Al) units reached its maximum at 48 hours, after which it decreased together with the further consumption of Q^0, Q^1 and Q^2 species to form more Q^4(3Al) or Q^3(1Al) and Q^4(2Al) structures. The reaction products formed between 48 hours and 240 hours are normally amorphous according to the XRD results. Compared with Q^4(4Al), these products are richer in Si, belonging to so-called "gel 2" [36,59]. The later formation of Si-rich gels compared with Al-rich products is due to the preferential dissolution of Al over Si from the precursor in the early stages of reaction, with delayed dissolution of Si occurring as the curing time was increased

[25]. However, it is noteworthy that the "very" Si-rich gels consisting of $Q^4(0Al)$, $Q^4(1Al)$ and $Q^4(2Al)$ units were rarely formed due to the high alumina content in MK. In this period, more Si was incorporated in the framework, therefore Al was mainly connected with -O-Si-, rather than -OH. This explains why the signal of Al-OH in the FTIR spectra for sample 48h and 240h is not observed. The formation of Si-rich gel in this stage might result from the polymerization between Al-rich nuclei and Si-rich oligomers available in the interstitial solution [60].

3.2.4 Summation of the characterization results

Combining the characterization results obtained from FTIR, XRD and NMR, the reaction processes corresponding to different chemical deformation stages can be summarised as follows:

- During the first hours (before 8 hours) when MKG showed chemical shrinkage, the sample was mainly experiencing dissolution, with MK dissolved and small species produced.

- When the samples were cured for more than 8 hours, small species were consumed in favour of the formation of Al-rich products, which consist of a certain amount of (nano-) zeolites acting as nuclei for further polymerization. The formation of these (nano-) zeolites or gels was associated with the chemical expansion of the paste in the second stage.

- When the samples were cured for more than 48 hours, the Al-rich entities were reorganized and further polymerized with the silicate oligomers available in the interstitial solution to produce a Si-rich geopolymer network. During this stage, the MKG underwent chemical shrinkage.

Of course, these reaction processes occur to some extent simultaneously during geopolymerization, but individually they dominated in certain periods. The reaction processes summarised above are generally consistent with those reported in the literature [30–36], but just here the relationship between the reaction processes and the chemical deformations is built up.

3.3 Interpretation of the chemical deformations associated with different reaction processes

3.3.1 Chemical shrinkage caused by the dissolution of precursor

The volume change during the dissolution of 30 g MK in 1000 g alkali solution is measured to be -0.059 ml/g_{mk} (the detailed testing method is described in 2.2.3), meaning a volume decrease of 0.059 ml/g_{mk}. This volume reduction during dissolution of MK is in consistent with the chemical shrinkage measured for MKG in the first stage. However, the value 0.059 ml/g_{mk} is higher than the chemical shrinkage value which reached only 0.032ml/g_{mk} at 8 hours as shown in Fig.2. The higher volume reduction determined in the dissolution test is believed to be due to the higher extent of

dissolution of MK in a huge amount of activator than in paste. The very high liquid to solid ratio (1000 g/30 g) largely facilitate the dissolution of MK and in the meantime dilute the concentration of dissolved species so that polymerization among the dissolved species is eliminated. On the other hand, the chemical shrinkage of the MKG paste due to dissolution can be compensated by the chemical expansion occurred in the second stage (which will be elaborated in next section), thus the chemical shrinkage measured for the paste is much lower.

A rough theoretical estimation of the chemical shrinkage of the MKG in the dissolution process can also be made based on the density of MK and the molar volumes of $Si(OH)_4$ and $Al(OH)_4^-$ if we simplify the dissolving of MK as in equation 1. It is assumed that the MK is completely dissolved and the reaction products after dissolving are simply monomers.

$$(SiO_2)_{1.53} \cdot Al_2O_3 + 6.06\ H_2O + 2OH^- \longrightarrow 1.53\ Si(OH)_4 + 2Al(OH)_4^- \qquad (1)$$

The SiO_2/Al_2O_3 ratio of the reactive part of MK is 1.53, so the chemical formula of MK is expressed as $(SiO_2)1.53 \cdot Al_2O_3$. The molar volumes of $Si(OH)_4$ and $Al(OH)_4^-$ are important for the calculation. According to the experimental data from literature or from the database provided by the sodium silicate and sodium aluminate producers [61–67], the molar volumes of $Si(OH)_4$ and $Al(OH)_4^-$ in similar chemical environments with this study normally fell in the range of 58.0-59.6 ml/mol and 40.6-44.7 ml/mol, respectively. Therefore, the molar volumes of $Si(OH)_4$ and $Al(OH)_4^-$ are herein assigned to be 58.68 and 42.30, respectively. The molar volume of H_2O is 18 ml/mol, while the one for OH^- is assigned to be -4.7 ml/mol according to the reference [68]. The density of the amorphous part of MK was 2.08 g/ml. The chemical deformation associated with equation 1 can be accordingly calculated as shown in Table 4.

Table 4

Calculation of chemical deformation of equation 1.

Reactants or reaction products	Moles	Mass	Density or molar volume	Volume
MK $(SiO_2)_{1.53} \cdot Al_2O_3$	1	193.8 g	2.08 g/ml	88.90 ml
H_2O	6.06	109.08 g	18 ml/mol	109.08 ml
OH^-	2	34	-4.7 ml/mol	-9.4 ml
$Si(OH)_4$	1.53	146.88 g	58.68 ml/mol	89.78 ml
$Al(OH)_3$	2	156 g	42.3 ml/mol	84.6 ml
Volume change			-18.47 ml	
Chemical deformation			-0.095 ml/g_{mk}	

The chemical shrinkage calculated based on equation 1 is 0.095ml/g_{mk}, which is not identical to the measured chemical shrinkage of MKG in the first stage (0.032ml/g_{mk}). This is because the reaction shown by equation 1 is an ideal and simplified case. In real geopolymerization, the species after dissolving are not only monomers, and even monomers may polymerize after they are released from the precursor [69]. Moreover, the chemical expansion in the second stage will compensate part of the chemical shrinkage that occurred in the first hours. Nonetheless, 0.095 ml/g_{mk} obtained from the rough calculation is at least in the same order of magnitude as the chemical shrinkage measured by experiment.

3.3.2 Chemical expansion caused by the formation of Al-rich (nano-) zeolites

It has been shown in Section 3.2 that the chemical expansion of MKG in the second stage is closely related to the formation of Al-rich products. These products are found to consist of a certain amount of zeolites and/or secondary building units/fragments of zeolites. The similar molecular structures of these products to zeolites result in lower local densities of these products compared with monomers or small oligomers. Before polymerization, silicate and aluminate species (monomers or small oligomers) suspend in interstitial solution. The volume that monomers or small oligomers occupy is close to the sum of their van der Waals molecular volumes [70]. When these species are polymerized to form crystalline structures like zeolites, pores within these frameworks are created and occupy a certain amount of volume. Some of these intracrystalline pores are too small to be accessible to guest molecules even as small and polar as water [71]; the other ones like intracrystalline channels or cavities may be big enough to be accessible to water, but the packing density of the water molecules within these spaces is less than in bulk solution [72]. In this case, the total volume occupied by these crystalline units together with the water molecules produced during polymerization consists of not only the intrinsic volume of the atoms forming solid and liquid but also the occluded volume. For example, the porosity of LTA zeolite ($Na_{12}(AlO_2)_{12}(SiO_2)_{12} \cdot 27H_2O$, as shown in Fig.8) is 77.7%, but the volume that could be occupied by liquid within the structure is only 43.3%, meaning 34.5% of the volume within LTA is occluded [73]. The occluded volume within the crystalline structures is the main reason why the (nano-) zeolites and water produced from polymerization occupy a larger volume than the reactants (monomers or oligomers). In addition, due to the existence of occluded volume, part of the interstitial water that cannot stay within the framework will be expelled out [71]. Accordingly, experimental evidence was found as shown in Fig. 9 with a certain amount of water or pore solution expelled out from the MKG paste at curing age of 16 hours. It has to be noted that the expelling of liquid observed at this stage was not due to bleeding which mainly happens for freshly mixed samples.
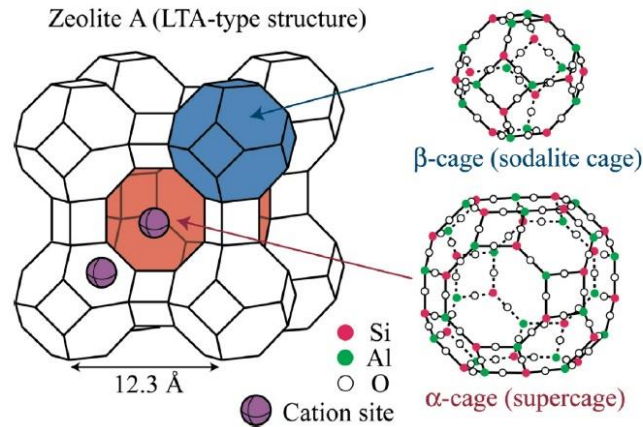
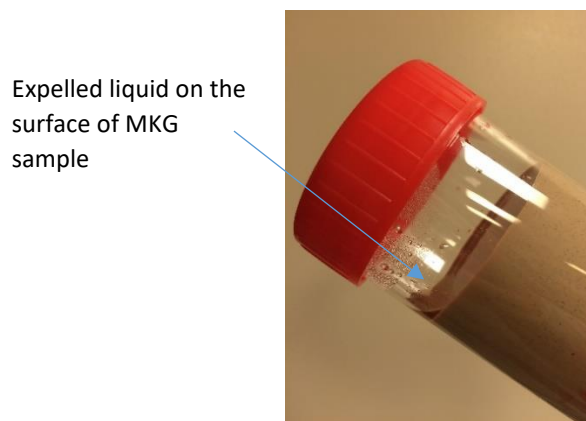Fig. 8. Schematic representation of LTA zeolite structure [74].

Expelled liquid on the surface of MKG sample

Fig.9. Expelled liquid observed on the surface of MKG cured for 16 hours.

Using LTA ($Na_{12}(AlO_2)_{12}(SiO_2)_{12} \cdot 27H_2O$) as an example, the chemical deformation of the formation of LTA can be roughly calculated as shown in equation 2, assuming the reactants are purely monomers. The molar volume of NaOH is assigned to 6.23mol/ml according to the concentration of the solution [75–78]. $Si(OH)_4$ comes from either the dissolving of MK or the activator and $Al(OH)_3$ comes only from the dissolving of MK. The chemical deformation during formation of LTA type zeolite is shown in Table 5.

1.53 $Si(OH)_4$ + 2$Al(OH)_4^-$ + 0.47 $Si(OH)_4$ + 2 Na^+

$\longrightarrow$ 0.167 $Na_{12}(AlO_2)_{12}(SiO_2)_{12} \cdot 27H_2O$ + 3.5 H_2O (2)
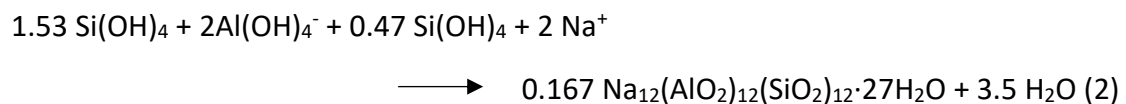
Table 5

Calculation of chemical deformation of equation 2.

Reactants or reaction products	moles	Mass	Density or molar volume	Volume
$Si(OH)_4$	1.53+0.47	192 g	58.68 ml/mol	117.36 ml
$Al(OH)_4^-$	2	190 g	42.3 ml/mol	84.6 ml
Na^+	2	46 g	-1.2 ml/mol	-2.4 ml

$Na_{12}(AlO_2)_{12}(SiO_2)_{12} \cdot 27H_2O$	0.167	365 g	1125.7 ml/mol [73]	187.99 ml
H_2O	3.5	63 g	18 ml/mol	63 ml
Volume change			51.43 ml	
Chemical deformation			0.265 ml/g_{mk}	

It can be seen that the reaction forming LTA type zeolite from monomers shows chemical expansion, which is evidence for the previous inference. According to the available data of zeolites in [71], it can be calculated that the formation of different kinds of zeolites (e.g. zeolite LTA, faujasite, phillipsite, etc) from monomers can generate different amounts of chemical expansions, but never chemical shrinkage, due to the large intrazeolitic porosities and the large occluded volumes in these zeolites. In the MKG paste studied here, the products formed in the second stage may be only secondary building units or fragments of zeolites which may not be observed by X-ray, but the (nano-) crystalline structures of these products can already induce chemical expansion.

The chemical expansion processed within MK geopolymerization and the expelling of pore solution observed from experiment are very interesting phenomena, in comparison with the monotonic chemical shrinkage and uptake of water during hydration of OPC. This information will be useful to explore the influences of the expelling of pore solution on engineering properties (such as efflorescence, autogenous shrinkage and drying shrinkage) of geopolymers in future research.

3.3.3 Chemical shrinkage caused by the formation of Si-rich gel

In zeolites, a large amount of volume in the intracrystalline pores is occluded or inaccessible to water due to their small pore sizes which are mainly in nm or Å level [71]. By contrast, the pores formed during the formation of amorphous Si-rich gels are mainly gel pores or capillary pores, whose sizes are in nm to μm level [79,80]. In these pores, the status of water molecules are just like in bulk solution and occluded volume would rarely exist. Therefore, the local density of geopolymer gels should be denser than the zeolites. Supports for this view can be found in [81], which, through atomistic simulation, proved that the geopolymer gel has lower porosity and thus higher density than crystalline zeolites like sodalite. In this case, reduction of volume would occur when the (nano-) zeolites were decomposed and polymerized/reorganized to form space-filling geopolymer gels. This may explain why MKG experienced a chemical shrinkage process in the late age of geopolymerization.

Similar to section 3.3.1 and 3.3.2, the volume change associated with the formation of geopolymer gels can be approximately calculated based on the density or molar volume data of the gels. Due to the amorphous nature of the gels, it is hard to directly determine the densities of the gels by experiments. Nonetheless, according to the methods presented by Myers et al. [68] and Thomas et al. [82], the density of a geopolymer gel with a given chemical formula can be calculated according to [68]. Since the Si-rich gels formed in the third stage are mainly $Q^4(3Al)/Q^3(1Al)$ and $Q^4(2Al)$ with an overall Si/Al ratio around 1.5, here we assume the chemical formula of one of

the main gels formed in this stage is $Na \cdot AlO_2 \cdot 1.5SiO_2 \cdot H_2O$. The density of gel $Na \cdot AlO_2 \cdot 1.5SiO_2 \cdot H_2O$ can be calculated to be 2.64 g/ml according to [68,82]. We then assume that the formation of gel $Na \cdot AlO_2 \cdot 1.5SiO_2 \cdot H_2O$ is from the polymerization between (nano-) LTA type zeolite with incorporation of silicate monomers, as shown by Eq. (3). It is noticed that the reactions occurred in reality would be more complex than shown by Eq. (3). The gels may not be formed directly from the (nano-) crystals. The (nano-) crystals may experience first decomposition and the species from the decomposition then react with the silicate monomers to form gels. The chemical deformation associated with Eq. (3) is shown in Table 6.
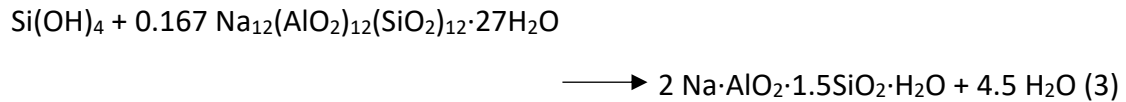
$$Si(OH)_4 + 0.167\ Na_{12}(AlO_2)_{12}(SiO_2)_{12} \cdot 27H_2O$$

$$\longrightarrow 2\ Na \cdot AlO_2 \cdot 1.5SiO_2 \cdot H_2O + 4.5\ H_2O \quad (3)$$

Table 6

Calculation of chemical deformation of equation 3.

Reactants or reaction products	moles	Mass	Density or molar volume	Volume
$Si(OH)_4$	1	96 g	58.68 ml/mol	58.68 ml
$Na_{12}(AlO_2)_{12}(SiO_2)_{12} \cdot 27H_2O$	0.167	365 g	1125.7 ml/mol	187.99 ml
$Na \cdot AlO_2 \cdot 1.5SiO_2 \cdot H_2O$	2	380 g	2.64 g/ml	143.94 ml
H_2O	4.5	81 g	1 g/ml	81 ml
Volume change			- 21.73 ml	
Chemical deformation			-0.112 ml/g_{mk}	

As shown in Table 6, the reorganization from LTA type zeolite to geopolymer gel with a Si/Al of 1.5 generates chemical shrinkage, which is coherent with the experiment results. The value 0.112ml/g_{mk} is much higher than the experimental chemical shrinkage, i.e., 0.015ml/g_{mk} in the third stage. That is because not all the reaction products in the second stage are crystals like LTA, and 0.015ml/g_{mk} is just the chemical shrinkage occurred till 2 weeks, when the reactions are far from finished. Despite the difference in values, the calculation helps to explain why the formation of NASH gel would induce chemical shrinkage.

3.4 Summary and final discussion

Based on the experimental results and the theoretical interpretations, clear connections between the chemical deformations and the reaction processes have been established and explained. A conceptual model can be summarised in Fig.10. The geopolymerization of MK with the activator of NaOH and Na_2SiO_3 experienced three stages of reaction processes and therefore three stages of chemical deformations. In the very early age, MKG paste showed chemical shrinkage due to the continuous dissolution of the precursor to form monomers or small oligomers. In the second stage, MKG paste experienced chemical expansion during the formation of Al-rich products which contain a certain amount of (nano-) zeolites. During this period, a certain amount of pore solution was expelled out from the paste. It will be very interesting to

further explore the influences on engineering properties of MKG systems of this expelling of pore solution, which is essentially different from the uptake of water in conventional cement hydration. In the final stage, the Al-rich products were reorganized and polymerized with the silicate oligomers to form amorphous Si-rich gels, during which MKG pastes showed chemical shrinkage again.
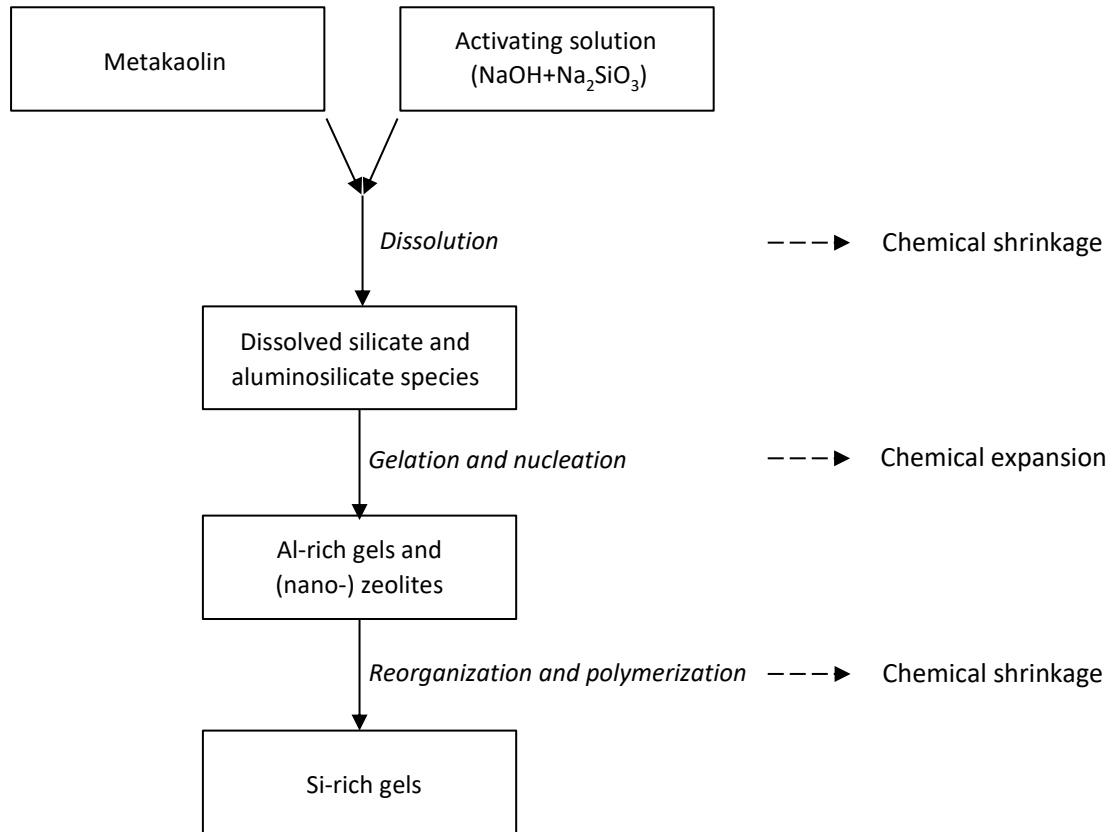
Fig.10. Reaction processes and chemical deformations of geopolymerization.

The reaction sequence presented in Fig.10 is similar to what had been shown in [83] but is modified to include the nucleation process, through which (nano-) zeolites would form, into the reaction pathways based on the XRD and FTIR results. Aluminate monomers are not included in the products after dissolution because they would react with silicate species immediately after it is formed [69].

The conceptual model presented in Fig.10 contributes to an in-depth understanding of the mechanism of MKG chemical deformation, which is crucial for estimating the driving force of bulk deformations of geopolymers. Of course, Fig.10 only describes the typical situation of activating MK by NaOH and Na_2SiO_3 at room temperature. If the raw material properties, type of activator and curing conditions are changed, the chemical deformation values will also change. Nonetheless, the principles proposed by this study will still work. For example, if one type of MK with higher density is used as precursor, the chemical shrinkage of the paste in the first stage would be smaller, due to the small volume reduction during dissolution; if pure NaOH is used as activator or if elevated temperature is used for curing, the chemical expansion in the second

stage is supposed to increase, due to the higher tendency to form zeolites in high PH or high-temperature condition [50]. Further research on quantitative analysis and prediction of chemical deformation is absolutely helpful, which may be done by the combination of thermodynamic modeling and experimental work.

4. Conclusions

This research presents an in-depth investigation on the chemical deformation of MK based geopolymer. For the first time, it is found that the chemical deformation MKG cured at ambient temperature doesn't show monotonic chemical shrinkage like OPC based binder. MKG experiences three stages of chemical deformations, including an initial chemical shrinkage, a followed-up chemical expansion and a chemical shrinkage again in the final stage. Through systemic experimental studies, clear relationships were found between the reaction processes and chemical deformations. Furthermore, a conceptual model of the reaction processes and corresponding chemical deformation is proposed based on experimental results and theoretical calculations.

This study provides important insights into the chemical deformation associated with geopolymerization, which will play a fundamental role for further understanding, controlling and even utilizing deformation behaviour (especially the autogenous deformation) of geopolymers in engineering applications. In addition, the conceptual model of the chemical deformation proposed in this study can be adapted for different geopolymer mixtures under various curing conditions in future researches. In the meantime, this study provides a new (volumetric) aspect to study geopolymerization especially the reaction processes before a final geopolymer gel is formed.

Acknowledgment

References

[1]   J. Davidovits, geopolymer and geopolymeric materials, J. Therm. Anal. 35 (1989) 429–441. doi:10.1017/CBO9781107415324.004.

[2]   K.L. Scrivener, R.J. Kirkpatrick, Innovation in use and research on cementitious material, Cem. Concr. Res. 38 (2008) 128–136. doi:10.1016/J.CEMCONRES.2007.09.025.

[3]   J.L. Provis, Geopolymers and other alkali activated materials: why, how, and what?, Mater. Struct. 47 (2014) 11–25. doi:10.1617/s11527-013-0211-5.

[4]   J.L. Provis, J.S.J. Van Deventer, Geopolymers: structures, processing, properties and industrial applications, Woodhead, Cambridge, UK, 2009.

[5]   K. Arbi, M. Nedeljković, Y. Zuo, G. Ye, A Review on the Durability of Alkali-Activated Fly Ash/Slag Systems: Advances, Issues, and Perspectives, Ind. Eng. Chem. Res. 55 (2016) 5439–5453. doi:10.1021/acs.iecr.6b00559.

[6]   M.C.G. Juenger, F. Winnefeld, J.L. Provis, J.H. Ideker, Advances in alternative cementitious binders, Cem. Concr. Res. 41 (2011) 1232–1243. doi:10.1016/j.cemconres.2010.11.012.

[7]   Z. Li, M. Nedeljkovic, Y. Zuo, G. Ye, Autogenous shrinkage of alkali-activated slag-fly ash pastes, in: 5th Int. Slag Valoris. Symp., Leuven, 2017: pp. 369–372.

[8]   Y. Ma, G. Ye, The shrinkage of alkali activated fly ash, Cem. Concr. Res. 68 (2015) 75–82. doi:10.1016/j.cemconres.2014.10.024.

[9]   Z. Li, P. Gao, G. Ye, Experimental study on autogenous deformation of metakaolin based geopolymer, in: 2nd Int. RILEM/COST Conf. Early Age Crack. Serv. Cem. Mater. Struct., Brussels, 2017: pp. 209–214.

[10]   D. FENG, A. Mikuni, Y. HIRANO, R. KOMATSU, K. Ikeda, Preparation of Geopolymeric Materials from Fly Ash Filler by Steam Curing with Special Reference to Binder Products, J. Ceram. Soc. Japan. 113 (2005) 82–86. doi:10.2109/jcersj.113.82.

[11]   F. Puertas, T. Amat, A. Fernández-Jiménez, T. Vázquez, Mechanical and durable behaviour of alkaline cement mortars reinforced with polypropylene fibres, Cem. Concr. Res. 33 (2003) 2031–2036. doi:10.1016/S0008-8846(03)00222-9.

[12]   Z. Zuhua, Y. Xiao, Z. Huajun, C. Yue, Role of water in the synthesis of calcined kaolin-based geopolymer, Appl. Clay Sci. 43 (2009) 218–223. doi:10.1016/j.clay.2008.09.003.

[13]   A. Mobili, A. Belli, C. Giosuè, T. Bellezze, F. Tittarelli, Metakaolin and fly ash alkali-activated mortars compared with cementitious mortars at the same strength class, Cem. Concr. Res. 88 (2016) 198–210. doi:10.1016/j.cemconres.2016.07.004.

[14]   O.M. Jensen, P.F. Hansen, Autogenous deformation and RH-change in

perspective, Cem. Concr. Res. 31 (2001) 1859–1865. doi:10.1016/S0008-8846(01)00501-4.

[15] P. Lura, O.M. Jensen, K. Van Breugel, Autogenous shrinkage in high-performance cement paste: An evaluation of basic mechanisms, Cem. Concr. Res. 33 (2003) 223–232. doi:10.1016/S0008-8846(02)00890-6.

[16] A.J. Allen, J.J. Thomas, H.M. Jennings, Composition and density of nanoscale calcium-silicate-hydrate in cement., Nat. Mater. 6 (2007) 311–316. doi:10.1038/nmat1871.

[17] A. Neville, Neville On Concrete, An Exam. Issues Concr. Pract. (2003) 531.

[18] C. Shi, D. Roy, P. Krivenko, Alkali-activated cements and concretes, CRC press, 2006.

[19] B. EN, 196-2 Methods of testing cement-Part 2: Chemical analysis of cement, Br. Stand. Institution, London. (2005).

[20] H. Justnes, E. Sellevold, B. Reyniers, D. Van Loo, A. Van Gemert, F. Verboven, D. Van Gemert, Chemical shrinkage of cement pastes with plasticizing admixtures, Nord. Concr. Res. 24 (2000) 39–44.

[21] M. Bouasker, P. Mounanga, P. Turcry, A. Loukili, A. Khelidj, Chemical shrinkage of cement pastes and mortars at very early age: Effect of limestone filler and granular inclusions, Cem. Concr. Compos. 30 (2008) 13–22. doi:10.1016/j.cemconcomp.2007.06.004.

[22] G. Sant, P. Lura, J. Weiss, Measurement of Volume Change in Cementitious Materials at Early Ages: Review of Testing Protocols and Interpretation of Results, Transp. Res. Rec. 1979 (2006) 21–29. doi:10.3141/1979-05.

[23] K. Scrivener, R. Snellings, B. Lothenbach, A practical guide to microstructural analysis of cementitious materials, Crc Press, 2016.

[24] P. Duxson, J.L. Provis, G.C. Lukey, F. Separovic, J.S.J. Van Deventer, ^{29}Si NMR study of structural ordering in aluminosilicate geopolymer gels, Langmuir. 21 (2005) 3028–3036. doi:10.1021/la047336x.

[25] B. Walkley, R. San Nicolas, M.-A. Sani, J.D. Gehman, J.S.J. van Deventer, J.L. Provis, Phase evolution of $Na2O-Al_2O_3-SiO_2-H_2O$ in synthetic aluminosilicate binders, Dalt. Trans. 45 (2016) 5521–5535. doi:10.1039/C5DT04878H.

[26] C. Ruiz-Santaquiteria, J. Skibsted, Identification of Reactive Sites in Calcined Kaolinite and Montmorillonite from a Combination of Chemical Methods and Solid-State NMR Spectroscopy, in: Calcined Clays Sustain. Concr., Springer, 2018: pp. 404–408.

[27] S.A. Bernal, J.L. Provis, B. Walkley, R. San Nicolas, J.D. Gehman, D.G. Brice, A.R. Kilcullen, P. Duxson, J.S.J. Van Deventer, Gel nanostructure in alkali-activated binders based on slag and fly ash, and effects of accelerated carbonation, Cem. Concr. Res. 53 (2013) 127–144. doi:10.1016/j.cemconres.2013.06.007.

[28] E. ichi Tazawa, S. Miyazawa, T. Kasai, Chemical shrinkage and autogenous shrinkage of hydrating cement paste, Cem. Concr. Res. 25 (1995) 288–292. doi:10.1016/0008-8846(95)00011-9.

[29] T.C. Powers, Absorption of Water by Portland Cement Paste during the Hardening Process, Ind. Eng. Chem. 27 (1935) 790–794. doi:10.1021/ie50307a011.

[30] P. Steins, A. Poulesquen, O. Diat, F. Frizon, Structural evolution during geopolymerization from an early age to consolidated material, Langmuir. 28 (2012) 8502–8510. doi:10.1021/la300868v.

[31] V.D. Glukhovsky, Soil silicate articles and structures, Russ. Budivel'nyk Publ. Kiev. (1967).

[32] J. Davidovits, Geopolymer Chemistry & Applications, 4 th, Institut Géopolymère, Saint-Quentin, France, 2015.

[33] J.C. Swanepoel, C.A. Strydom, Utilisation of fly ash in a geopolymeric material, Appl. Geochemistry. 17 (2002) 1143–1148.

[34] L. Weng, K. Sagoe-Crentsil, Dissolution processes, hydrolysis and condensation reactions during geopolymer synthesis: Part I-Low Si/Al ratio systems, J. Mater. Sci. 42 (2007) 2997–3006. doi:10.1007/s10853-006-0820-2.

[35] J.L. Provis, P. Duxson, J.S.J. van Deventer, G.C. Lukey, The role of mathematical modelling and gel chemistry in advancing geopolymer technology, Chem. Eng. Res. Des. 83 (2005) 853–860. doi:10.1205/cherd.04329.

[36] P. Duxson, A. Fernández-Jiménez, J.L. Provis, G.C. Lukey, A. Palomo, J.S.J. van Deventer, Geopolymer technology: the current state of the art, J. Mater. Sci. 42 (2007) 2917–2933. doi:10.1007/s10853-006-0637-z.

[37] Z. Zhang, H. Wang, J.L. Provis, F. Bullen, A. Reid, Y. Zhu, Quantitative kinetic and structural analysis of geopolymers. Part 1. the activation of metakaolin with sodium hydroxide, Thermochim. Acta. 539 (2012) 23–33. doi:10.1016/j.tca.2012.03.021.

[38] W.K.W. Lee, J.S.J. van Deventer, Use of infrared spectroscopy to study geopolymerization of heterogeneous amorphous aluminosificates, Langmuir. 19 (2003) 8726–8734. doi:Doi 10.1021/La026127e.

[39] W.R. Taylor, Application of infrared spectroscopy to studies of silicate glass structure: Examples from the melilite glasses and the systems Na_2O-SiO_2 and Na_2O-Al_2O_3-SiO_2, Proc. Indian Acad. Sci. - Earth Planet. Sci. 99 (1990) 99–117. doi:10.1007/BF02871899.

[40] H. Watling, Spectroscopy of concentrated sodium aluminate solutions, Appl. Spectrosc. 52 (1998) 250–258. doi:10.1366/0003702981943310.

[41] J.L. Bass, G. Turner, Anion distributions in sodium silicate solutions. Characterization by ^{29}Si NMR and infrared spectroscopies, and vapor phase osmometry, J. Phys. Chem. B. 101 (1997) 10638–10644.

doi:10.1021/jp9715282.

[42]   A. Gédéon, P. Massiani, F. Babonneau, Zeolites and Related Materials: Trends Targets and Challenges (SET): 4th International FEZA Conference, 2-6 September 2008, Paris, France, Elsevier, 2008.

[43]   J. Osswald, K.T. Fehr, FTIR spectroscopic study on liquid silica solutions and nanoscale particle size determination, J. Mater. Sci. 41 (2006) 1335–1339.

[44]   I. Garcia-Lodeiro, A. Fernandez-Jimenez, D.E. Macphee, I. Sobrados, J. Sanz, A. Palomo, Stability of synthetic calcium silicate hydrate gels in presence of alkalis, aluminum, and soluble silica, Transp. Res. Rec. 2142 (2010) 52–57.

[45]   P. Wang, Q. Xu, Materials Research Methods, Beijing: Science Press, 2005.

[46]   F. Puertas, M. Palacios, H. Manzano, J.S. Dolado, A. Rico, J. Rodríguez, A model for the CASH gel formed in alkali-activated slag cements, J. Eur. Ceram. Soc. 31 (2011) 2043–2056.

[47]   C. a Rees, J.L. Provis, G.C. Lukey, J.S.J. van Deventer, Attenuated total reflectance fourier transform infrared analysis of fly ash geopolymer gel aging., Langmuir. 23 (2007) 8170–8179. doi:10.1021/la700713g.

[48]   N. V Chukanov, Infrared spectra of mineral species: extended library, Springer Science & Business Media, 2013.

[49]   W. Mozgawa, M. Król, K. Barczyk, FT-IR studies of zeolites from different structural groups, Chemik. 65 (2011) 671–674.

[50]   J.L. Provis, G.C. Lukey, J.S.J. Van Deventer, Do geopolymers actually contain nanocrystalline zeolites? a reexamination of existing results, Chem. Mater. 17 (2005) 3075–3085. doi:10.1021/cm050230i.

[51]   A. Bauer, G. Berger, Kaolinite and smectite dissolution rate in high molar KOH solutions at 35 and 80 C, Appl. Geochemistry. 13 (1998) 905–916.

[52]   W. Sun, Y. Zhang, W. Lin, Z. Liu, In situ monitoring of the hydration process of K-PS geopolymer cement with ESEM, Cem. Concr. Res. 34 (2004) 935–940.

[53]   M. Rowles, B. O'connor, Chemical optimisation of the compressive strength of aluminosilicate geopolymers synthesised by sodium silicate activation of metakaolinite, J. Mater. Chem. 13 (2003) 1161–1165.

[54]   Z. Yunsheng, S. Wei, L. Zongjin, Composition design and microstructural characterization of calcined kaolin-based geopolymer cement, Appl. Clay Sci. 47 (2010) 271–275. doi:10.1016/j.clay.2009.11.002.

[55]   C.A. Rees, J.L. Provis, G.C. Lukey, J.S.J. van Deventer, The mechanism of geopolymer gel formation investigated through seeded nucleation, Colloids Surfaces A Physicochem. Eng. Asp. 318 (2008) 97–105. doi:10.1016/j.colsurfa.2007.12.019.

[56]   C.K. Yip, G.C. Lukey, J.S.J. van D. Dean, Effect of Blast Furnace Slag Addition on Microstructure and Properties of Metakaolinite Geopolymeric Materials, Adv.

Ceram. Matrix Compos. IX. 153 (2012) 187–209. doi:10.1002/9781118406892.ch13.

[57] V. Kahlenberg, H. Bohn, Crystal structure of hexagonal trinepheline; a new synthetic NaAlSiO 4 modification, Am. Mineral. 83 (1998) 631–637.

[58] B. Walkley, R. San Nicolas, M.A. Sani, G.J. Rees, J. V. Hanna, J.S.J. van Deventer, J.L. Provis, Phase evolution of C-(N)-A-S-H/N-A-S-H gel blends investigated via alkali-activation of synthetic calcium aluminosilicate precursors, Cem. Concr. Res. 89 (2016) 120–135. doi:10.1016/j.cemconres.2016.08.010.

[59] A. Fernández-Jiménez, A. Palomo, I. Sobrados, J. Sanz, The role played by the reactive alumina content in the alkaline activation of fly ashes, Microporous Mesoporous Mater. 91 (2006) 111–119. doi:10.1016/j.micromeso.2005.11.015.

[60] A. Favier, G. Habert, N. Roussel, J.-B. d'Espinose de Lacaillerie, A multinuclear static NMR study of geopolymerisation, Cem. Concr. Res. 75 (2015) 104–109. doi:10.1016/j.cemconres.2015.03.003.

[61] PQ Corp, Typical property data for PQ liquid sodium silicates, Chem. Typ. Prop. Data PQ Corp. Hqrs. (2012).

[62] J.G. Reynolds, The Density of Aqueous Sodium Hydroxide- Sodium Aluminate Solutions : Data Review and Model Development, in: WM'06 Conf., 2006.

[63] J. Li, C.A. Prestidge, J. Addai-Mensah, Viscosity, density, and refractive index of aqueous sodium and potassium aluminate solutions, J. Chem. Eng. Data. 45 (2000) 665–671. doi:10.1021/je000025d.

[64] P. Sipos, A. Stanley, S. Bevis, G. Hefter, P.M. May, Viscosities and densities of concentrated aqueous NaOH/NaAl(OH)4 mixtures at 25 °C, J. Chem. Eng. Data. 46 (2001) 657–661. doi:10.1021/je000347h.

[65] J.K. Hovey, C. Nguyen-trung, T. Peter R, Thermodynamics of aqueous uranyl ion: Apparent and partial molar heat capacities and volumes of aqueous uranyl perchlorate from 10 to 55°C, Geochim. Cosmochim. Acta. 53 (1989) 1503–1509. doi:10.1016/0016-7037(89)90233-0.

[66] B. Sanjuan, T.I.A. Molality, A. Molar, E. Section, Determination of the Partial Molar Volume of Al(OH)$^-$ at Infinite Dilution in Water at 25 °C, J. Chem. Eng. Data. (1988) 78–80.

[67] T. Ikkatai, N. Okada, K.K. Showa, Viscosity, specific gravity, and equilibrium concentration of sodium aluminate solutions, Extr. Metall. Alum. 1 (1963) 159–173.

[68] R.J. Myers, S.A. Bernal, J.L. Provis, A thermodynamic model for C-(N-)A-S-H gel: CNASH-ss. Derivation and validation, Cem. Concr. Res. 66 (2014) 27–47. doi:10.1016/j.cemconres.2014.07.005.

[69] L. Weng, K. Sagoe-Crentsil, Dissolution processes, hydrolysis and condensation

reactions during geopolymer synthesis: Part II-High Si/Al ratio systems, J. Mater. Sci. 42 (2007) 2997–3006. doi:10.1007/s10853-006-0820-2.

[70]   A. Bondi, van der Waals Volumes and Radii, J. Phys. Chem. 68 (1964) 441–451. doi:10.1021/j100785a001.

[71]   R.M. Barrer, Hydrothermal chemistry of zeolites, Academic press, 1982.

[72]   François-Xavier Coudert, Water nanodroplets confined in zeolite pores, Faraday Discuss. 141 (2009) 9–30. doi:10.1039/B816684F.

[73]   Q.H. Dirar, K.F. Loughlin, Intrinsic adsorption properties of CO2 on 5A and 13X zeolite, Adsorption. 19 (2013) 1149–1163. doi:10.1007/s10450-013-9543-2.

[74]   Takahito Nakano, Abnormality and spin orbit interaction in strong magnetic field magnetization process of K cluster in zeolite A (In Japanese), Osaka Univ. Low Temp. Cent. 145 (2009) 2–9.

[75]   J.M. Simonson, R.J. Ryther, Volumetric properties of aqueous sodium hydroxide from 273.15 to 348.15 K, J. Chem. Eng. Data. 34 (1989) 57–63. doi:10.1021/je00055a017.

[76]   R.H. Perry, D.W. Green, J.O. Maloney, Perry's Chemical Engineers' Handbook, 6th ed., McGraw-Hill Book Company, 1984.

[77]   W.M. Haynes, CRC handbook of chemistry and physics, CRC press, 2014.

[78]   G. Akerlof, P. Bender, The Density of Aqueous Solutions of Potassium Hydroxide, J. Am. Chem. Soc. 63 (1941) 1085–1088. doi:10.1021/ja01849a054.

[79]   J.L. Provis, J.S.J. Van Deventer, Alkali Activated Materials, 2014. doi:10.1007/978-94-007-7672-2.

[80]   C.E. White, D.P. Olds, M. Hartl, R.P. Hjelm, K. Page, Evolution of the pore structure during the early stages of the alkali-activation reaction: an *in situ* small-angle neutron scattering investigation, J. Appl. Crystallogr. 50 (2017) 61–75. doi:10.1107/S1600576716018331.

[81]   F. Lolli, H. Manzano, J.L. Provis, M.C. Bignozzi, E. Masoero, Atomistic Simulations of Geopolymer Models: The Impact of Disorder on Structure and Mechanics, ACS Appl. Mater. Interfaces. 10 (2018) 22809–22820. doi:10.1021/acsami.8b03873.

[82]   J.J. Thomas, A.J. Allen, H.M. Jennings, Density and water content of nanoscale solid C-S-H formed in alkali-activated slag (AAS) paste and implications for chemical shrinkage, Cem. Concr. Res. 42 (2012) 377–383. doi:10.1016/j.cemconres.2011.11.003.

[83]   J.L. Provis, J.S.J. van Deventer, Geopolymerisation kinetics. 1. In situ energy-dispersive X-ray diffractometry, Chem. Eng. Sci. 62 (2007) 2309–2317. doi:10.1016/j.ces.2007.01.027.